International Journal for Numerical Methods in Fluids
Int. J. Numer. Meth. Fluids **26**: 217–234 (1998)

A NUMERICAL STUDY OF TURBULENT LINE PUFFS VIA THE RENORMALIZATION GROUP (RNG) $k-\epsilon$ MODEL

J.H.W. LEE[a,*] AND G.Q. CHEN[b]

[a] *Department of Civil Engineering, University of Hong Kong, Hong Kong, China*
[b] *Centre for Environmental Sciences, Peking University, Beijing 100871, China*

SUMMARY

The time evolution of a line puff, a turbulent non-buoyant element with significant momentum, is studied using the renormalization group (RNG) $k-\epsilon$ model. The numerical results show that the puff motion is characterized by a vortex pair flow; the computed flow details and scalar mixing characteristics can be described by self-similar relations beyond a dimensionless time of around 30. The added mass coefficient of the puff motion is found to be approximately unity. The predicted puff flow and mixing rate are substantially similar to those obtained from the standard $k-\epsilon$ model and are well supported by experimental data. The computed scalar field reveals significant secondary concentration peaks trailing behind in the wake of the puff. The present results suggest that the overall mixing rate of a puff is primarily determined by the large-scale motion and that streamline curvature probably plays a minor role. © 1998 John Wiley & Sons, Ltd.

KEY WORDS: Puffs and thermals; turbulence modelling; jets and plumes; environmental fluid mechanics; vortex flow; added mass.

1. INTRODUCTION

Puff flow is recognized as one of the fundamental phenomena in environmental fluid mechanics [1]. It is often reasoned that the flow in the vertical section of a bent-over jet in crossflow is similar to that of a line puff [1–3]. In an early experimental study [4] the observed puff spreading rate, measured by the ratio of the puff front location to the maximum horizontal radius, exhibited great scatter, differing from that of line thermals by a factor of two [1]. Little quantitative detail on the flow was given and the passive scalar field was not studied. Subsequently, visual trajectory and limited tracer concentration measurements in the bent-over phase of a momentum-dominated buoyant jet in crossflow have been made [5,6]. However, partly owing to the difficulty of isolating such an asymptotic flow regime, the measured dilution rates also exhibited considerable scatter. Later, the bent-over jet in crossflow was treated analytically by Yih [7], assuming a constant puff velocity component and negligible diffusion in the direction of crossflow. Employing Prandtl's free shear layer model for turbulence closure, a self-similar solution was derived for the asymptotic stage; a two-term

* Correspondence to: Department of Civil Engineering, University of Hong Kong, Hong Kong.

Contract grant sponsor: Hong Kong Research Grants Council
Contract grant sponsor: National Science Foundation of China

CCC 0271–2091/98/020217–18$17.50 *Received May 1996*
© 1998 John Wiley & Sons, Ltd.

approximation of the series solution was given. Although the mixing process was not studied, the flow field was illustrated for a value of dimensionless eddy viscosity for which the approximation is valid. More recently, the puff problem was studied by numerical simulation of the flow and mixing using the standard two-equation k–ϵ model as a first approximation and by experimental measurement of the scalar concentration field in an advected line puff [3]. The numerical study revealed a loss of initial impulse due to pressure interaction; the associated added mass coefficient was found to be approximately unity. From the results therein it can be shown that the value adopted in Yih's analysis is unrealistically small (by a factor of 50).

The stream function contours obtained by the standard k–ϵ model [3] (henceforth referred to as the LRW study) show clearly a vortex pair flow and the existence of regions with high strain rate in the puff. As is well known, the standard k–ϵ model has one important shortcoming, namely that a spuriously high generation rate of turbulence energy can be predicted around points or regions of high strain rate. This excess of turbulence energy creates high levels of turbulent viscosity. As the spurious turbulence energy is advected downstream in the rear of the puff, the high turbulent viscosity may overpredict mixing and suppress related flow details. To explore further the effect of alternative turbulence models on puff mixing, we study herein the time evolution of a line puff by employing the renormalization group (RNG) model. Building on the LRW study, our objective is to study (i) the effect of streamline curvature (high strain rate) on the overall puff flow and mixing characteristics and (ii) the sensitivity of some flow details, in particular the trailing vorticity in the puff rear, to an alternative turbulence model hypothesis.

We perform a numerical experiment on a turbulent line puff in very much the same way as if one were doing a laboratory experiment. A finite momentum is imparted to a two-dimensional marked patch of incompressible fluid and the mixing of such a line puff with the otherwise stagnant surrounding fluid is investigated. Within the eddy viscosity approximation the two-equation RNG model is adopted to solve for the turbulence kinetic energy and its dissipation rate. The numerical solutions are then compared with experimental data and discussed.

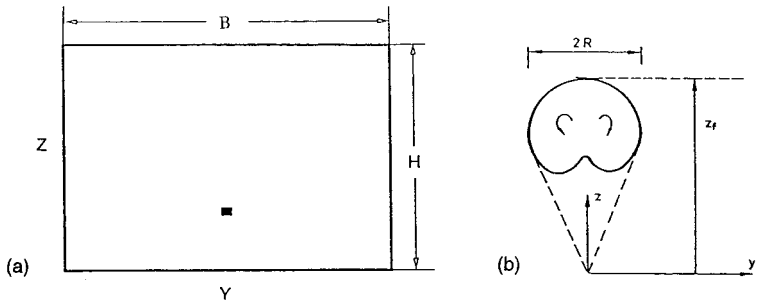

Figure 1. Turbulent line momentum puff: (a) numerical experiment on a line puff in an incompressible fluid—an initial impulse is applied in the positive z-direction to the marked square patch (of length L_0) inside a water tank; (b) definition of puff front and radius

© 1998 John Wiley & Sons, Ltd.

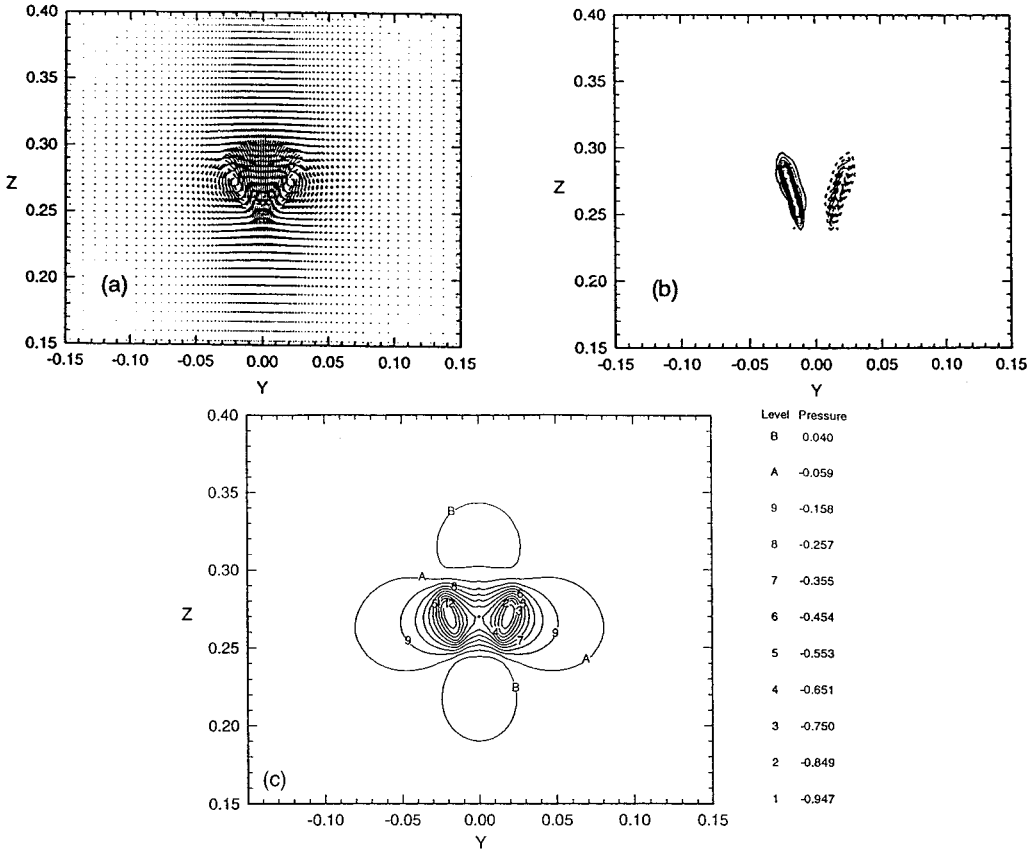

Figure 2. Initial flow generated at $t^* = 0.5$: (a) velocity field—maximum velocity magnitude is 0.724 m s^{-1}; (b) vorticity contours—all 24 equally spaced contours are concentrated into two kernels. (c) Pressure field p^* at $t^* = 0.5$—maximum and minimum values are 0.040 and -0.947 respectively

2. FORMULATION AND THEORY

2.1. Numerical experiment

Figure 1(a) shows a volume of water initially at rest in a tank of width B and H. At time $t = 0$ a significant impulse M_0 in the vertical (z) direction is applied to a square patch of fluid (of length L_0) initially labelled at uniform passive scalar concentration C_0 and located sufficiently far away from the solid boundaries. The momentum source gives rise to significant vorticity and a turbulent mass of fluid which is advected in the direction of the imparted momentum while mixing with the ambient fluid. The motion and characteristics of this puff (the 'coloured' patch) (Figure 1(b)) are investigated.

In all the results reported herein, the following parameters are adopted: $B = 1.2$ m, $H = 0.9$ m, $M_0 = 0.001712$ m^3 s^{-1}, $L_0 = 0.04$ m. The impulse is applied on the domain $D_0 = (y_{l0}, y_{r0}) \times (z_{b0}, z_{f0}) = (-0.02, 0.02) \times (0.245, 0.285)$. Both the tank dimensions and initial puff size are comparable with those of previous experiments on line thermals and puffs.

© 1998 John Wiley & Sons, Ltd.

2.2. Governing equations

We take the Reynolds-averaged equations for constant-density incompressible flow,

$$\frac{\partial U_i}{\partial x_i} = 0, \tag{1}$$

$$\frac{\partial U_i}{\partial t} + U_j \frac{\partial U_i}{\partial x_j} = -\frac{1}{\rho}\frac{\partial p}{\partial x_i} + \frac{\partial \tau_{ij}}{\partial x_j}, \tag{2}$$

where U_i is the fluid velocity in the y- or z-direction, ρ is the density, p is the dynamic pressure and τ_{ij} is the stress tensor, equal to the sum of the viscous and Reynolds stresses. The eddy viscosity model (Boussinesq hypothesis) provides the following expression for the stresses:

$$\tau_{ij} = \nu_{\text{eff}}\left(\frac{\partial U_j}{\partial x_i} + \frac{\partial U_i}{\partial x_j}\right) - \frac{2}{3}k\delta_{ij}, \tag{3}$$

where the effective viscosity ν_{eff} is equal to the sum of the molecular viscosity ν and the turbulent viscosity ν_{t}, i.e.

$$\nu_{\text{eff}} = \nu + \nu_{\text{t}}. \tag{4}$$

The RNG k–ϵ model [8] adopts the following relations for turbulence closure:

$$\nu_{\text{eff}} = \nu\left[1 + \sqrt{\left(\frac{C_\mu}{\nu}\right)}\frac{k}{\sqrt{\epsilon}}\right]^2, \tag{5}$$

$$\frac{\partial k}{\partial t} + U_i\frac{\partial k}{\partial x_i} = \nu_{\text{t}}S^2 - \epsilon + \frac{\partial}{\partial x_i}\alpha_{\text{p}}\nu_{\text{t}}\frac{\partial k}{\partial x_i}, \tag{6}$$

$$\frac{\partial \epsilon}{\partial t} + U_i\frac{\partial \epsilon}{\partial x_i} = C_{1\epsilon}\frac{\epsilon}{k}\nu_{\text{t}}S^2 - C_{2\epsilon}\frac{\epsilon_2}{k} - R + \frac{\partial}{\partial x_i}\alpha_{\text{p}}\nu_{\text{t}}\frac{\partial \epsilon}{\partial x_i}, \tag{7}$$

where $C_\mu = 0.0845$, k is the turbulence kinetic energy (TKE), ϵ is referred to as the dissipation rate (DR) of k and α_{p} is the inverse Prandtl number for turbulent transport as computed via the equation

$$\left|\frac{\alpha_{\text{p}} - 1.3929}{0.3929}\right|^{0.6321}\left|\frac{\alpha_{\text{p}} + 2.3929}{3.3929}\right|^{0.3679} = \frac{\nu}{\nu_{\text{eff}}}. \tag{8}$$

The rate-of-strain term R is given by

$$R = \frac{C_\mu\eta^3(1 - \eta/\eta_0)}{1 + \beta\eta^3}\frac{\epsilon^2}{k}, \tag{9}$$

where $\eta = Sk/\epsilon$, $\eta_0 = 4.38$ and $S^2 = 2S_{ij}S_{ij}$ is the modulus of the rate-of-strain tensor expressed as $S_{ij} = \frac{1}{2}(\partial U_i/\partial x_j + \partial U_j/\partial x_i)$. RNG theory gives values of the constants $C_{1\epsilon} = 1.42$ and $C_{2\epsilon} = 1.68$. Equation (8) shows that α_{p} tends to a constant value of 1.39 for fully turbulent flow at high Reynolds number; its value is reduced for low-Reynolds-number flow and approaches unity in the limit of laminar flow. In addition to the flow equations, the study of puff characteristics necessitates the calculation of a passive scalar field from the conservation equation

$$\frac{\partial C}{\partial t} + U_j\frac{\partial C}{\partial x_j} = \frac{\partial}{\partial x_j}\left(\frac{\nu_{\text{t}}}{Sc_{\text{t}}}\frac{\partial C}{\partial x_j}\right), \tag{10}$$

© 1998 John Wiley & Sons, Ltd.

where Sc_t stands for the turbulent Schmidt number, equal to $1/\alpha_p$ in RNG theory. The RNG $k-\epsilon$ model differs from the commonly used standard $k-\epsilon$ model and its variants in several ways. Constants and functions in the RNG model are evaluated by rigorous theory and not by empiricism. The model is therefore much more generally applicable without modification. Low-Reynolds-number effects are included in RNG theory, permitting laminar-like behaviour to be predicted and hence making it more applicable to the partly turbulent characteristics of puff flow. The reduced value of $C_{2\epsilon}$, as compared with the value of 1.9 in the standard model, has the interesting consequence of decreasing both the rate of production of k and the rate of dissipation of ϵ, leading to smaller values of v_{eff}. The new term R is related to the strain rate for treatment of non-equilibrium effects and flows in the rapid distortion limit. In regions of small strain rate the term R tends to increase v_{eff} somewhat, but v_{eff} is still typically smaller than its value in the standard theory. However, in regions of large strain rate the sign of R is changed and v_{eff} is decreased much more.

The vorticity equation for an incompressible homogeneous fluid is

$$\frac{\partial \tilde{\omega}_i}{\partial t} + U_j \frac{\partial \tilde{\omega}_i}{\partial x_j} = \tilde{\omega}_j \frac{\partial \tilde{u}_i}{\partial x_j} + v \frac{\partial^2 \tilde{\omega}_i}{\partial x_j \partial x_j}, \tag{11}$$

where $\tilde{u}$ and $\tilde{\omega}$ stand for the instantaneous velocity and vorticity respectively. After substituting related Reynolds decompositions into this equation and taking ensemble averages of all terms, we obtain a governing equation for the vorticity of the turbulent mean flow, Ω, as follows:

$$\frac{\partial \Omega_i}{\partial t} + U_j \frac{\partial \Omega_i}{\partial x_j} = -\frac{\partial}{\partial x_j}(\overline{u_j \omega_i}) + \overline{\omega_j \frac{\partial u_i}{\partial x_j}} + \Omega_j \frac{\partial U_i}{\partial x_j} + v \frac{\partial^2 \Omega_i}{\partial x_j \partial x_j}, \tag{12}$$

where u and ω stand for the fluctuating velocity and vorticity respectively. In the limit of two-dimensional turbulent flow the second and third terms on the right-hand side of the equation, which account for the effect of vortex stretching, disappear. The remaining first term $(\partial/\partial x_j)(\overline{u_j \omega_i})$ has no counterpart in the equation for instantaneous vorticity (Equation (11)). As a transport 'divergence' analogous to the Reynolds stress term in the momentum equation, it is due to mean transport of the fluctuating vorticity ω_i through its interaction with the fluctuating velocity u_j. For turbulent flows at large Reynolds number this mechanism can be dominant, because the vorticity fluctuation is much larger than the mean vorticity. For puff flow this argument can be supported by another form of the mean vorticity equation obtained by taking the curl of the momentum Equation (2) with the eddy viscosity assumption. It can be shown from this form of the vorticity equation that, besides the mechanism of vorticity diffusion, the inhomogeneity of the eddy viscosity distribution furnishes another mechanism for vorticity change. The latter mechanism can be significant, as the eddy viscosity varies substantially across the puff. That is why the vorticity field of the Reynolds-averaged puff flow computed in the LRW study could be quite different from that deduced from classical vorticity dynamics [9] assuming constant viscosity. It is then not surprising that certain formal interpretations which are applicable only to the instantaneous vorticity (see e.g. Reference [10]) are irrelevant to the mean vorticity; this point will be discussed further.

2.3. Initial and boundary conditions

By virtue of the symmetry assumption, the numerical solution is sought for only half of the flow domain, i.e. $y \geq 0$. At solid boundaries the non-slip condition is imposed. On the line of symmetry, $y = 0$, the conditions $\partial W/\partial y = 0$ and $V = 0$ are imposed, where W stands for the

© 1998 John Wiley & Sons, Ltd.

vertical velocity; the normal gradients of all other variables are similarly set to zero. The fluid properties are taken as those of water, i.e. $\rho = 10^3$ kg m^{-3} and $\nu = 10^{-6}$ m^2 s^{-1}. At $t = 0$, zero values of horizontal velocity V and pressure are prescribed. The vertical velocity and scalar concentration are given the values $W_0 = 1.07$ m s^{-1} (according to M_0) and $C_0 = 1$ inside the marked patch and zero elsewhere. The values of k and ϵ for the patch are assumed to be 0.0176 m^2 s^{-2} and 0.0509 m^2 s^{-3} respectively, corresponding to an eddy viscosity estimated by a free shear model $\nu_t = \alpha_\nu W_0 L_0$, with $\alpha_\nu \sim 0.01$. For numerical reasons, negligibly small initial values of (k, ϵ) are given for the non-turbulent region outside the initial impulse such that $\nu_t < 0.001\nu$. As will be seen from the numerical results below, the solution in the asymptotic stage of the puff is rather insensitive to the initial values of k and ϵ assumed over a reasonable range.

2.4. Similarity relations

As the flow in the enclosed system is entirely driven by the nominal impulse, the variation puff characteristics can be written as $(W_c, C, L) = f(M_0, V_0, C_0, t)$, where W_c, C and L denote the characteristic vertical velocity, concentration and length respectively and $V_0 = L_0^2$ is the initial puff volume per unit length. An appropriate non-dimensionalized variable ϕ then depends only on the dimensionless time $t^* = t/t_c$, where $t_c = V_0^{3/2}/M_0$ is a characteristic time scale that measures the effect of the initial impulse geometry. Further, if the flow becomes self-similar, then for $t^* \gg 1$, dimensional analysis leads to

$$W_c \sim M_0^{1/3} t^{-2/3}, \tag{13}$$

$$z \sim M_0^{1/3} t^{1/3} \sim L, \tag{14}$$

where z is a characteristic location referred to from the initial source location, i.e. $z = Z - Z_{b0}$, and L is a characteristic dimension of the puff. Conservation of passive scalar also implies

$$\frac{C_0}{C} \sim \frac{M_0^{2/3} t^{2/3}}{V_0}. \tag{15}$$

These relations indicate that the puff Reynolds number Re and the circulation around one half of the puff, Γ, both $\sim W_c L$, decrease slowly as $\sim t^{-1/3}$. The above relations will be used to test the self-similarity of the numerical solution.

3. NUMERICAL SOLUTION

3.1. Computational procedure and details

The governing equations are solved numerically using the finite difference method [11] as embodied in the code FLUENT [12]. The equations are discretized on a non-staggered grid on which Cartesian velocities and other variables are defined at the centres of control volumes. The quadratic upwind interpolation (QUICK) approximation of Leonard [13] is used for spatial discretization. A first-order-accurate unconditionally stable implicit scheme is used for time discretization, with all spatial derivatives and other terms treated in a fully implicit manner. At each time step the discretized equations are solved iteratively using the SIMPLEC algorithm for velocity–pressure correction [14]. In all calculations no underrelaxation of pressure is required, while a factor of 0.8 is adopted for velocities and other variables. Convergence is declared when the normalized residuals are less than 5×10^{-4}.

© 1998 John Wiley & Sons, Ltd.

A 63×146 (y–z) orthogonal grid is used for this problem of simple geometry, with the initial source defined over 12×8 cells. The minimum grid dimensions are $\Delta y = 0.0017$ and $\Delta z = 0.005$; in the region of the growing puff the grid size is no more than 0.005 m. To obtain accurate solutions, up to 1000 time steps are used to march the solution to $t^* = 80$. In the initial stages, 300–500 iterations are required for convergence at each time step, but for $t^* > 3$, typically only 100–150 iterations suffice.

3.2. Flow field

The momentum source gives rise to a sharp velocity gradient (Figure 2(a)), leading to the formation of two vortices at the lateral edges of the puff (Figure 2(b)) and an unsymmetrical pressure distribution around the puff (Figure 2(c)). As a result of this pressure interaction, the puff vertical momentum $M_p = \int_p W \, dV$ drops to half of the nominal impulse at $t^* = 0.5$.

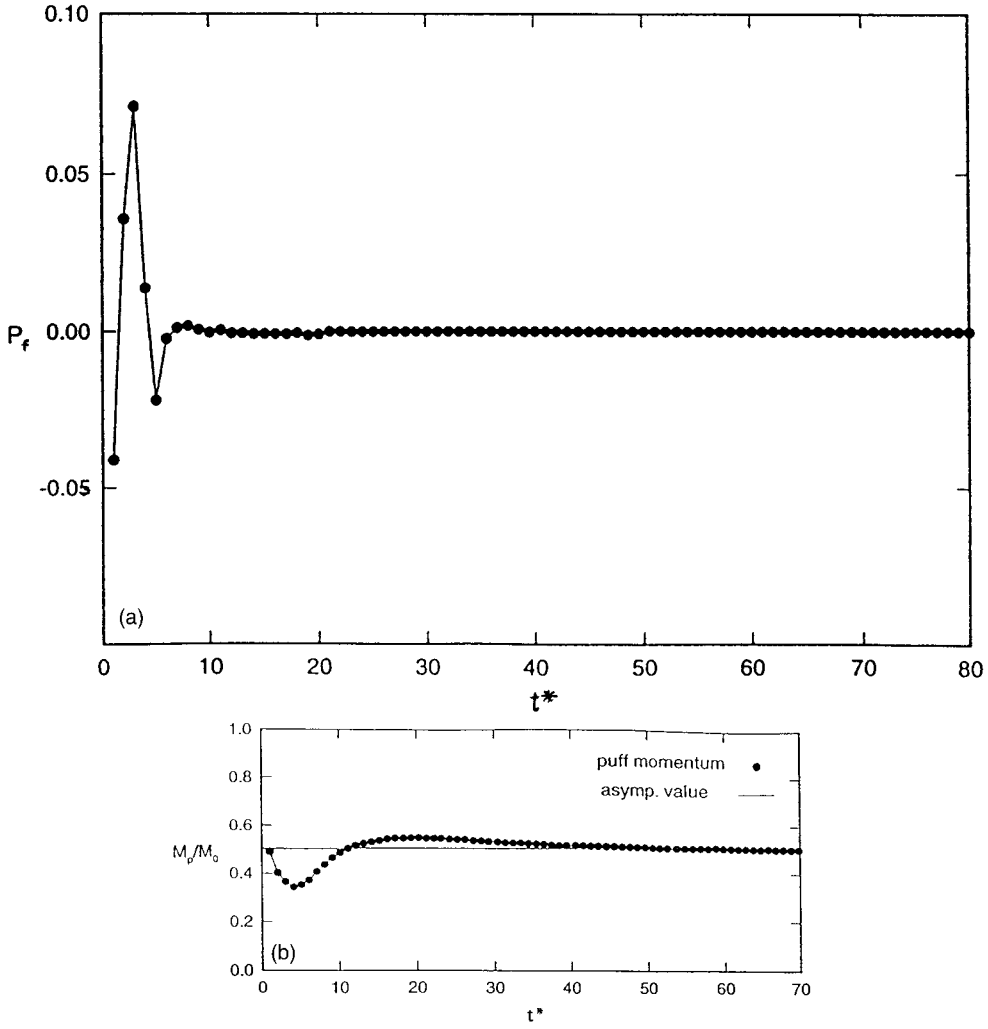

Figure 3. (a) Time variation of net pressure force (SI units) on puff. (b) Time variation of puff momentum M_p/M_0

© 1998 John Wiley & Sons, Ltd.

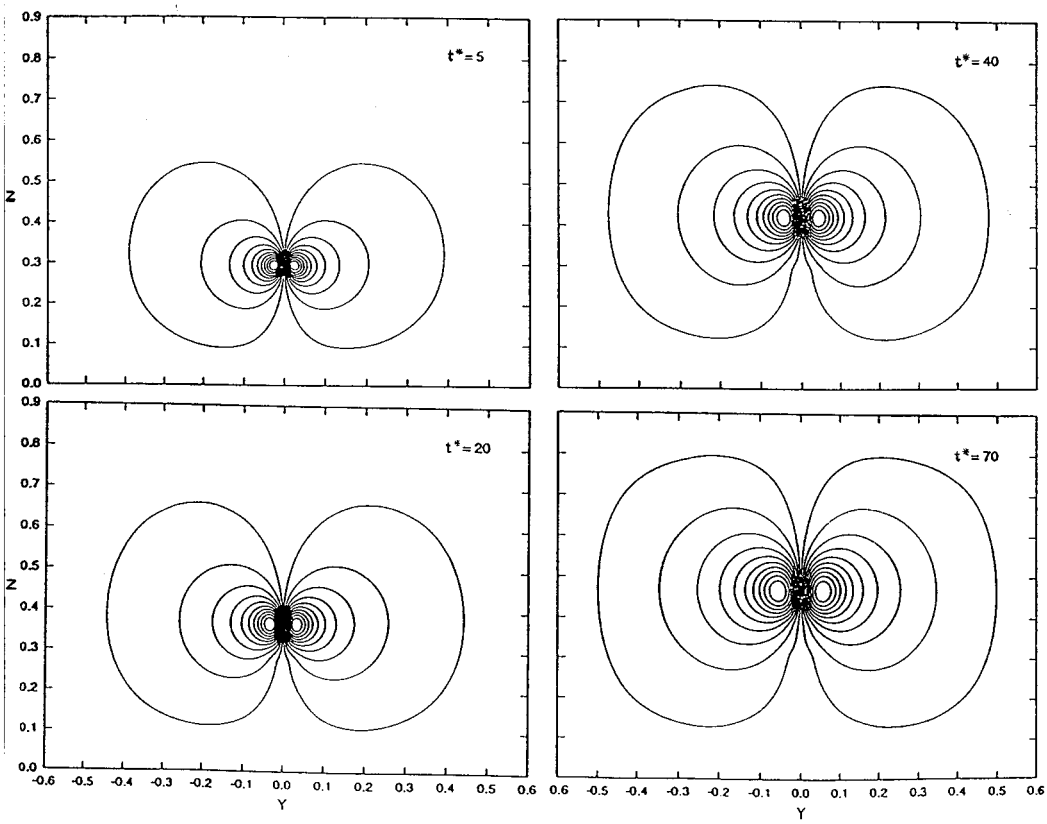

Figure 4. Computed streamlines—maximum normalized streamfunction $\Psi^*_m = 0.187$, 0.162, 0.155, 0.156 at $t^* = 5$, 20, 40, 70 respectively. Contour interval is $\Psi^*_m/10$

Figure 3(a) and 3(b) show the subsequent time variation of the net pressure force P_f acting on the puff (sum of pressures along top and bottom solid boundaries) and of M_p. It is seen that there are significant pressure fluctuations for $t^* < 10$; thereafter P_f drops to negligible values. The puff momentum initially decreases, then attains an asymptotic value of $0.5M_0$ beyond $t^* \sim 30$. Figures 4–7 show the computed flow and scalar fields at selected instants during $t^* = 5$–70. The following points may be made.

(i) The puff is characterized by a vortex-pair-like flow (Figure 4). As the flow develops, from $t^* \sim 20$ onwards, a clear inflection in the flow entering the puff from the rear can be noted, due to the appearance of a wake region of relative stagnation behind the rear of the main vortex pair flow (Figure 5), where the flow velocity is very small or zero. The shape of the flow field is well preserved for $t^* \geq 30$. The maximum magnitude of the normalized streamfunction $\Psi^* = \Psi/(W_m L)$ is equal to 0.187, 0.162, 0.155, 0.156 at $t^* = 5$, 20, 40, 70 respectively, where W_m is the maximum vertical velocity in the puff. The pressure field (not shown) is also approximately self-similar for $t^* \geq 30$, with the minimum pressure (non-dimensionalized by $\rho W_m^2/2$) given by $p^* = -0.947$ relative to initial zero value. P is positive in front of the puff, decreases to a negative minimum around the vortex centre and then increases to positive values at the rear of the puff.

(ii) The vorticity field (Figure 6) shows that the main body of the puff is surrounded at the rear by a significant vorticity layer and after $t^* \geq 20$ is followed by a vorticity spot, all with

© 1998 John Wiley & Sons, Ltd.

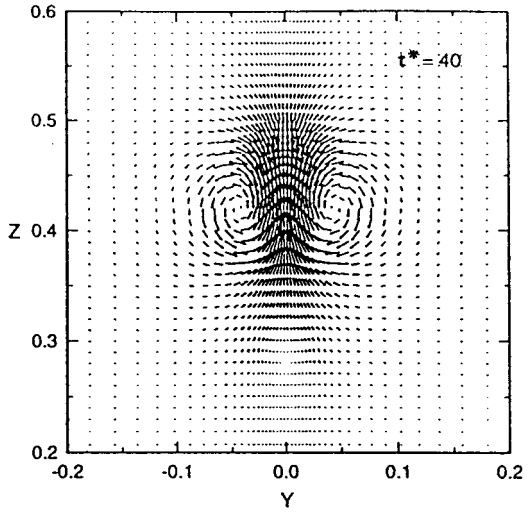

Figure 5. Computed velocity field with a wake region of stagnation

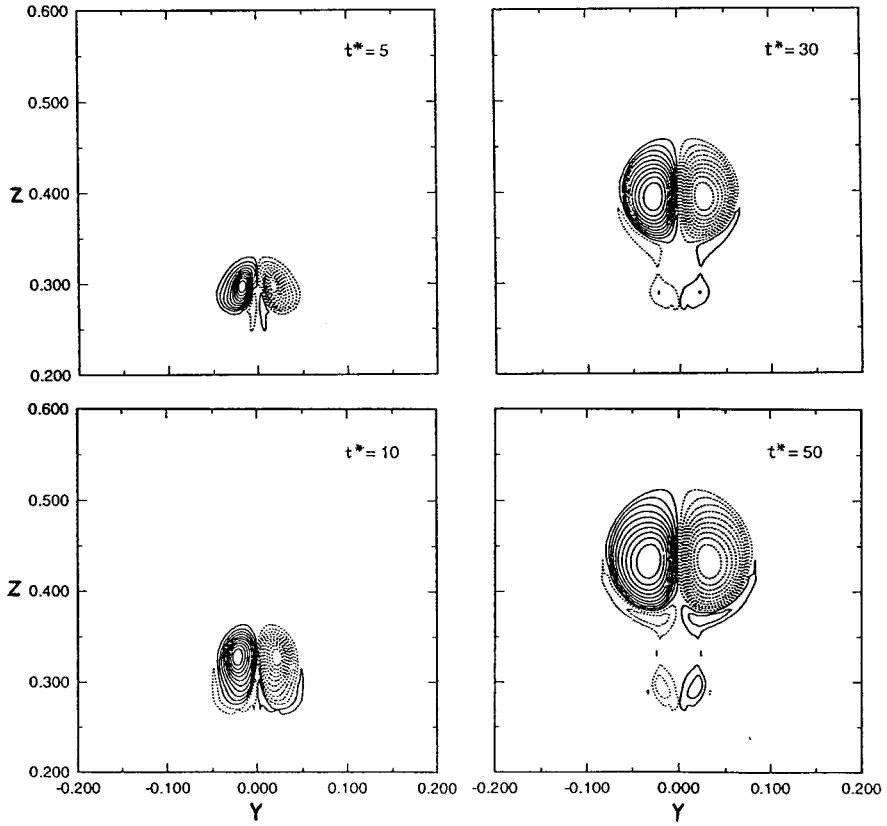

Figure 6. Computed vorticity field—maximum normalized vorticity (with increasing t^*) $\eta^*_m = 8.51, 7.10, 6.47, 6.37$. All contours with a negative vorticity value are shown as broken lines. Contour interval is $\eta^*_m/10$

© 1998 John Wiley & Sons, Ltd.

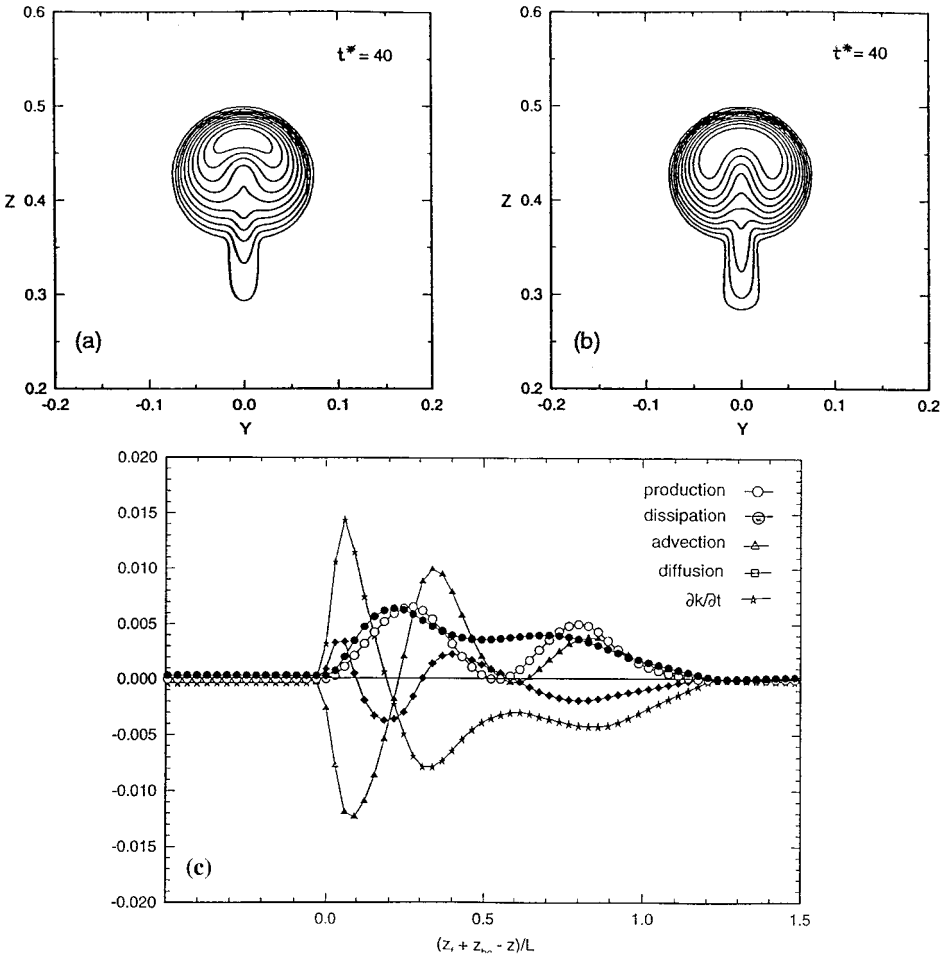

Figure 7. (a) Turbulence kinetic energy—$u_m/W_m = 0.36$. (b) Eddy viscosity—$\nu_{tm}/(W_m L) = 0.016$, $\nu_{tm}/\nu = 400$. (c) Relative magnitude of various terms in TKE budget of puff, plotted against distance relative to front of puff (along $y = 0$ at $t^* = 40$)

opposite orientation. It is remarkable that the spot is related to the relative stagnation of flow in the wake. Self-similarity is evident for $t \geq 30$, with the maximum normalized vorticity magnitude $\eta_m^* = \eta_m/(W_m/L) = 8.51$, 7.1, 6.47, 6.37 at the times shown. The magnitude of the maximum opposite vorticity is less than 0.28 of that of the maximum vorticity at the vortex centre in the self-similar stage.

(iii) The turbulence kinetic energy k and dissipation rate ϵ (hence turbulent viscosity ν_t) both display approximately preserved shapes for $t^* \geq 30$. Figure 7(a) shows that the region of high TKE is located towards the front of the puff, where large spatial gradients can be noted. The maximum values of k and ϵ are found at the same location, namely on the centre line and above the position of maximum vertical velocity. In the self-similar stage the maximum turbulence intensity is $u_m/W_m \approx 0.36$, where $k_m = \frac{3}{2} u_m^2$. In the main body of the puff the turbulent viscosity (Figure 7(b)), very similar in shape to k, varies spatially by about a factor of four, with the maximum value $\nu_t/(W_m L) = 0.016$ and $\nu_t/\nu \approx 400$. The characteristic length of

© 1998 John Wiley & Sons, Ltd.

the energy-containing motion, $l = C_\mu k^{3/2}/\epsilon$, is in the range (0.02–0.04)L. A lobe of non-negligible turbulence protruding into the wake of the puff can also be clearly noted. Figure 7(c) shows that the TKE balance of the puff is qualitatively similar to that of plane jets and wakes. The region of maximum production is found around regions of large velocity gradients, at the front of the puff, with significant production also towards the rear. While none of the terms in (6) is negligible, diffusion plays a relatively minor role as compared with advection. The front of the puff gains TKE by advection, while the converse is true towards the rear. The ratio of the total (integrated over the puff) production of TKE to the total dissipation rate, Pr/ϵ, varies from 0.92 at $t^* = 0.5$ to an asymptotic value of 0.68 at $t^* = 70$.

3.3. Passive scalar field

Figure 8 shows the computed passive scalar field. In the initial stages a symmetrical double-maxima pear-shaped structure is formed; the puff concentration maximum C_m, located around the vortex centre, can be as much as 1.4 times the maximum concentration C_c is along the centreline. This is in accord with previous observations in the bent-over phase of a jet in crossflow. While the double peaks can be noted only for $t^* < 20$, the symmetrical double-maxima structure transforms into a stretched-out kidney-shaped region of high concentration. The main body of the scalar field evolves to a rather round outline which becomes approximately self-similar for $t^* > 30$; thereafter a secondary concentration peak (with a magnitude as much as $0.5C_m$) develops in the puff rear, resulting in an oblong concentration appendix attached to the main body of the puff. The approximately asymptotic stage is reached when the puff has

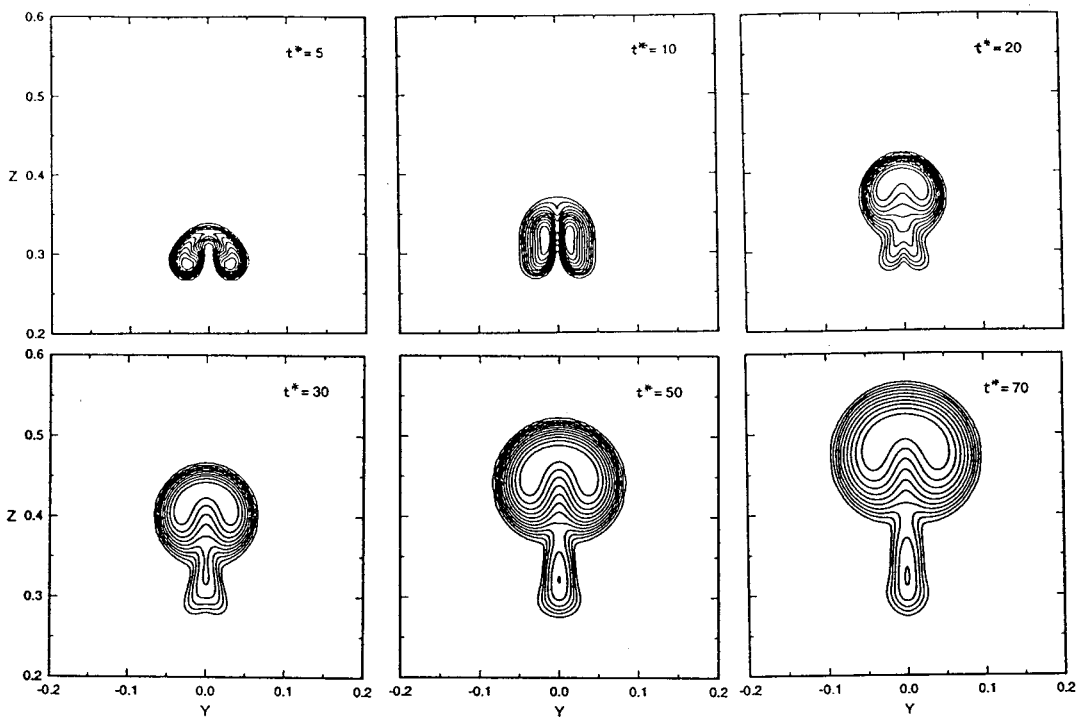

Figure 8. Computed passive scalar field

© 1998 John Wiley & Sons, Ltd.

Table I. Similarity relations derived from numerical solution (numbers refer to dimensionless coefficients of equations or ratios; $(k, \epsilon)_0$ in SI units)

	Parameter	RNG 1	RNG 2	RNG 3	SKE	Experiment
Initial conditions	k_0	0.0176	0.0056	0.0331	0.0176	
	ϵ_0	0.0509	0.0093	0.1260	0.0509	
Puff momentum	M_p/M_0	0.515	0.519	0.505	0.502	0.3[a]
Vertical velocity	$W_m = C_v M_0^{1/3} t^{-2/3}$	1.98	2.17	1.90	1.90	
Puff front	$z_f = nR$	3.16	3.08	3.09	2.92	2.6–5.7 [4]
Trajectory	$z_c = C_{2p} M_0^{1/3} t^{1/3}$	1.57	1.59	1.54	1.51	1.44 [16] 1.56 [3]
Length scale	$L = C_{4p} M_0^{1/3} t^{1/3}$	1.18	1.17	1.19	1.19	
Centre of mass	$L = C_{cm}\bar{z}$	0.90	0.85	0.95	0.95	
Scalar concentration	C_0/C_m $= C_{0m} M_0^{3/2} t^{2/3}/V_0$	0.722	0.737	0.741	0.648	
Scalar concentration	$C_0/C_m = C_{3p} z_c^2/V_0$	0.29	0.29	0.28	0.28	0.35 [3]
Centreline halfwidth	$b_{vc} = C_{1p} z_c$	0.349	0.330	0.355	0.290	0.276 [3]
	$W_m/\overline{W}$	3.61	3.47	3.73	3.62	
Circulation	$\Gamma/(\overline{W}L)$	2.58	2.50	2.71	2.72	
Momentum factor	$W_p/(\overline{W}L^2)$	0.63	0.63	0.64	0.67	
Turbulent viscosity	$\nu_t/(w_m L)$	0.016	0.015	0.017	0.015	
Turbulence intensity	u_m/W_m	0.36	0.35	0.37	0.36	
Prod./diss.	Pr/ϵ	0.68	0.72	0.64	0.54	
	C_m/C_c	1.02	1.01	1.02	1.01	1.00–1.56

[a]Vortex ring.

grown to larger than three times its initial size. The significant turbulent viscosities computed in the tail of the puff act to diffuse the scalar outwards into the appendix of the puff; the strong entrainment and the stagnation in the puff rear (Figure 5) help form the secondary concentration peak in the appendix.

Extensive tests have confirmed that the above general features are unrelated to the numerical procedure adopted. One lower-resolution simulation on a coarser 57×130 grid was made to validate the numerical accuracy. All the contour plots are very similar to the high-resolution results, and differences for all the non-dimensional parameters presented in Table I are limited to at most 4%. Combined with our previous extensive SKE simulation in the LRW study, we are reasonably assured that the numerical results represent an accurate simulation of the puff

© 1998 John Wiley & Sons, Ltd.

problem. In any case, the present results have captured the essentially self-similar flow during the time when most of the changes take place.

3.4. *Puff characteristics*

To investigate the self-similarity more fully, a large number of puff characteristics are computed at each time step. The maximum vertical velocity (Figure 9(a)) and maximum scalar concentration (Figure 9(b)) satisfy well the $-2/3$ similarity law (Equations (11) and (13)) for $t^* \geq 30$ and 20 respectively. Figures 9(c) and 9(d) show the variation of the vertical location of the puff front, z_f, with time and with the maximum horizontal radius R respectively. Both z_f and R are defined by the $0.01C_m$ contour. It can be seen that the puff front follows the 1/3 power law (Equation (12)) for $t^* \geq 20$. The puff front location varies linearly with R, with a slope of about three in the asymptotic stage. In experiments it is often expedient to measure a concentration transverse along the centreline. The location of the centreline concentration maximum C_c, z_c, also varies linearly with the halfwidth b_{vc}, defined by the $e^{-1}C_c$ points along the centreline. The similarity relations in the asymptotic stage $t^* > 30$ are summarized in Table I. Also shown are the ratio of the maximum to the mass-weighted average vertical velocity, W_m/W, and the circulation around one half of the puff, defined as $\Gamma = \int_0^H W(0,\ z)\,dZ$. The dimensionless results are virtually the same for a source with half of the strength assumed herein. Table I also shows that the mean flow properties of the self-similar puff are rather insensitive to the exact initial conditions of k and ε assumed within a reasonably wide range for the puff. Defining the puff by the $0.05C_m$ contour also produced negligible changes in the puff front and length relations.

4. DISCUSSION

In summary, the numerical results strongly support the concept of similarity for the puff flow; the transition to self-similarity lies in the range $t^* = 25$–30. The computed variation of the puff

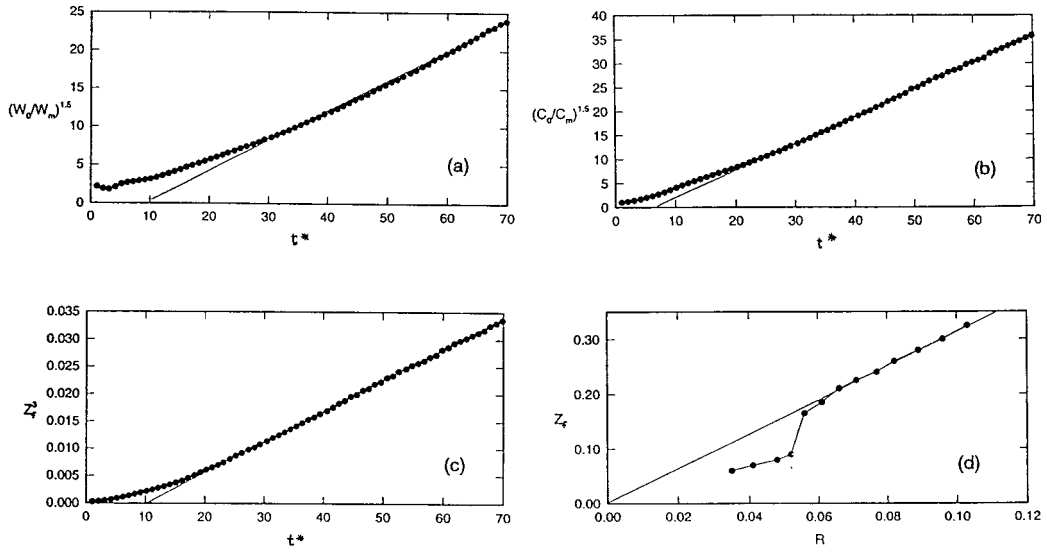

Figure 9. Time variation of puff properties: (a) maximum vertical velocity; (b) scalar concentration; (c) vertical location of puff front. (d) Puff front versus maximum horizontal radius. (See Table I for equations)

© 1998 John Wiley & Sons, Ltd.

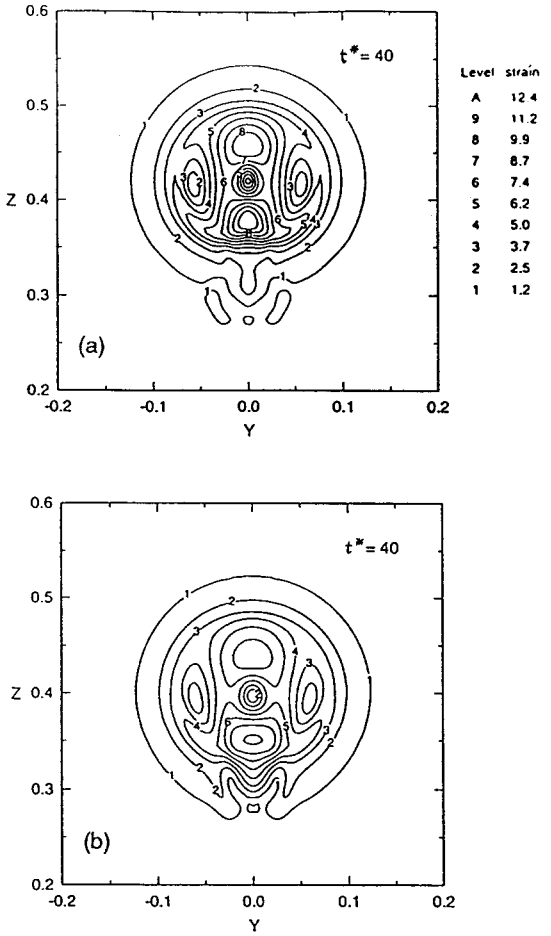

Figure 10. Computed fields of strain rate (SI units) distribution via (a) RNG model and (b) SKE model

front (Figures 9(c) and 9(d)) closely resembles the data of a previous experiment on line puffs [4]. In that experiment a short pulsed jet was generated by impulsively releasing water at excess head from a puffer into a tank. Although the initial momentum loss was not measured, the computed large pressure transients are in accord with the observed fluctuations in free surface level in the water tank and within the puffer. The substantial loss of nominal impulse is also supported by a study of vortex rings [15] in which the initial dimensionless momentum of the vortex ring was found to be about 0.3. The asymptotic value of 0.5 for the puff momentum, a fundamental property, can also be interpreted as an added mass of the unsteady puff motion [16,17], implying an added mass coefficient of unity. Half of the nominal impulse accounts for the approximately irrotational flow of the surrounding fluid set up by the moving puff.

The computed flow (Figure 4) is very similar to the observed mean fluid motion of the puff measured from particle tracks (Figure 6 of Reference [4]), although the flow inflection towards the rear of the puff cannot be noted in the experiment. For the measured flow the puff front/radius ratio is $n = 3.4$ and the flow outside the puff can be closely approximated by the potential flow due to a line doublet of strength $0.034 z_f^2 \, dz_f/dt$ per unit length. Our calculations show that $dz_f/dt \approx 0.45 W_m$. Using the observed n and our computed value of $W_m/\overline{W}$ (Table I),

© 1998 John Wiley & Sons, Ltd.

the observations imply a doublet strength $\mu = 0.64\overline{W}R^2$. On the other hand, analysis of the computed velocity field reveals that the outside flow can be closely approximated by that due to a doublet with $\mu = 0.63\overline{W}R^2$. This close agreement provides another quantitative confirmation of the numerical solution.

The computed spreading rate of the puff defined by z_f (Table I and Figure 1(b)), $n = 3.16$, lies within the observed range of 2.6–5.7. The large variation of the measured n could be related to the experimental difficulty of generating puffs of short pulse duration. The value of $n \approx 3$, the same as that observed by Tsang [18] in his study of thermals, appears to be more consistent with the observation that the puff flow is very similar to the line thermal flow.

Additional insights into the mixing of puffs can be gained from the present results. It can be shown that almost all the fluid presented to the puff cross-section is entrained into the puff, a result which can also be deduced from the experimental data of line thermals [19]. The entrainment coefficient α as used in models employing the entrainment assumption [17] can also be deduced to be 0.32, the use of which yields velocities close to that computed, $C_v = 1.90$–2.17. This value of α can be compared with the range of 0.25–0.67 obtained by Chu [16] in an analysis of previous data.

In Table I we also compare the puff trajectory and mixing rate with recent experiments of advected line puffs [3]. In those experiments an advected line puff was simulated by discharging a near-vertical round jet at zero excess horizontal momentum into a horizontal crossflow; the horizontal component of the initial jet velocity was made equal to the ambient velocity. Time-averaged scalar concentration measurements can be conveniently carried out in the cross-section of these puffs. The measured puff spreading rate as defined by the centreline halfwidth is 0.276 and the trajectory constant is $C_{2p} = 1.56$. Compared with the corresponding computed values of 0.349 and 1.57 respectively, the data lend support to the use of the RNG model for the study of puff mixing. In experiments the ratio of the maximum concentration to the maximum centreline concentration, C_m/C_c, varied in the range of 1–1.56. Taking a mean value of C_m/C_c of 1.3, the measured centreline dilution constant of 0.46 translates to a minimum dilution constant of 0.35. This compares with the computed puff mixing rate $C_{3p} = 0.29$ (Table I), where $C_0/C_m = C_{3p}z_c^2/V_0$. We also note that the dilution constant is sensitive to small errors in z_c.

5. COMPARISON WITH RESULTS FROM STANDARD k–ϵ (SKE) MODEL

As a comparison, a similar numerical experiment is performed using the standard k–ϵ model [20] for case 1, with the scalar concentration equation adopting a constant value of Sc_t equal to 0.75, as found appropriate for related computations [3,10]. As shown in Table I, the computed puff parameters are very close to those obtained by the RNG model. The notable exception is that the predicted spreading rate of centreline halfwidth by the standard model is noticeably smaller by about 20%. Although the overall mixing characteristics do not appear to be affected by the alternative turbulence model hypothesis, there are some notable differences in the computed flow field. Close examination of the standard model results (not shown) indicates a milder puff momentum response with time (possibly due to somewhat overpredicted diffusion); some flow details, such as the relative stagnation in the wake and the entrainment in the rear, are also somewhat suppressed. This smoothing effect can be clearly discerned in Figure 10, which compares the strain rate distributions computed by the two models. At the same time the strain rate from the RNG model is generally greater than that from the SKE model, corresponding to the smaller ν_{eff} computed by the RNG formulation. A

© 1998 John Wiley & Sons, Ltd.

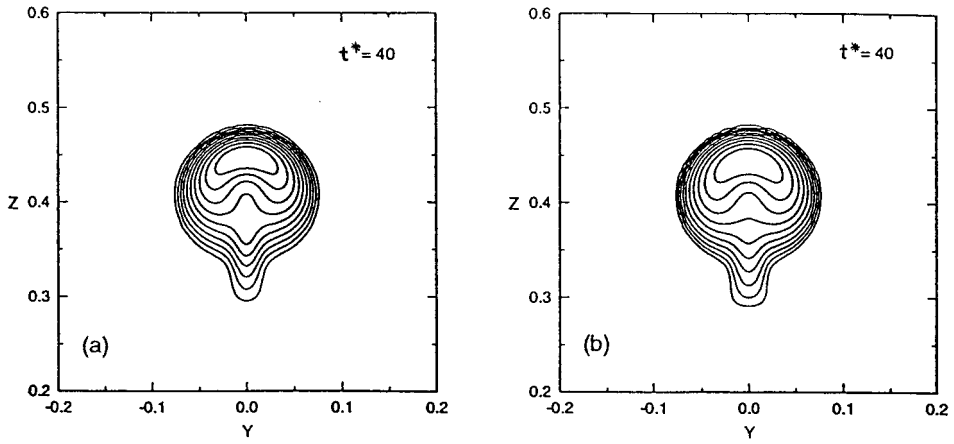

Figure 11. (a) Turbulence kinetic energy and (b) eddy viscosity via SKE model

similar tendency is true for the turbulence kinetic energy and turbulent viscosity, as shown in Figure 11.

The most significant difference between the predictions of the two models is in the passive scalar field (Figure 12). The scalar field contours obtained from the standard model, very similar to those reported in the LRW study, show a similar shape of the main puff body and

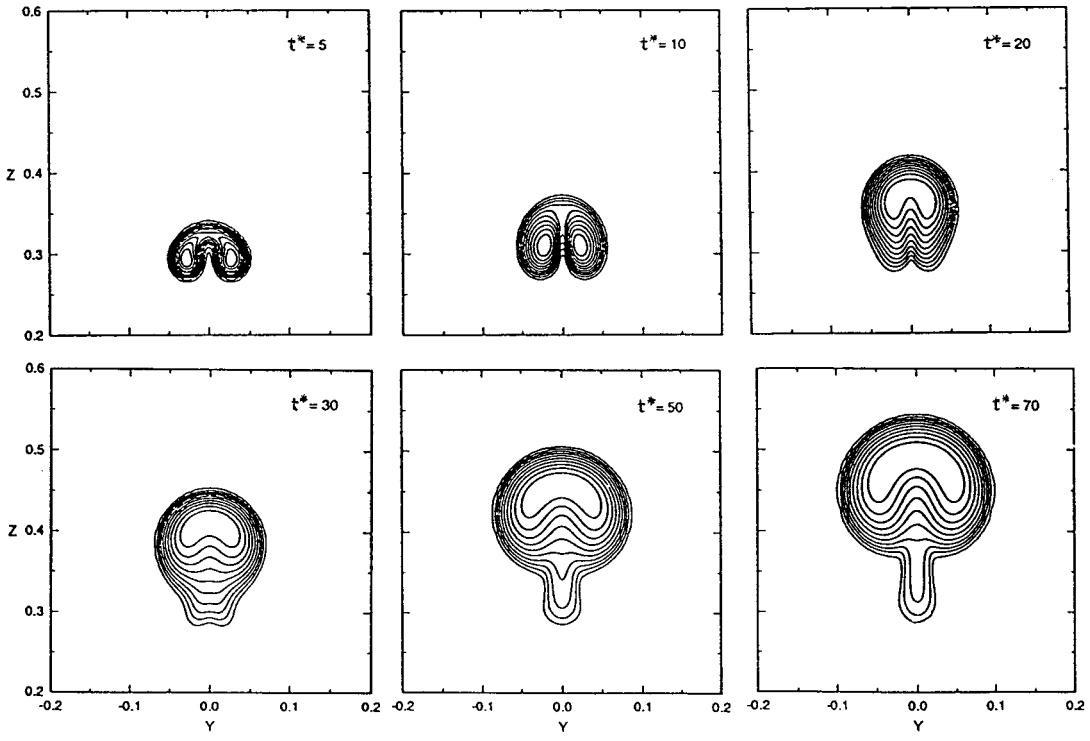

Figure 12. Computed passive scalar field via SKE model

© 1998 John Wiley & Sons, Ltd.

a small wake of insignificant concentration, possibly due to the weaker stagnation. On the other hand, the RNG model (Figure 8) shows a moving puff in which part of the 'coloured' patch is 'detrained' or deposited into a long appendix or wake, apparently due to the much stronger entrainment and stagnation found in that region.

6. CONCLUDING REMARKS

The mixing of unsteady line puffs has been studied using the renormalization group (RNG) model. The salient features of the predicted flow and scalar mixing rates are very similar to those obtained by the standard k–ϵ model and are well supported by experimental data. However, the predicted scalar field differs in detail from the measurements in the flow analogue of an advected puff. Some of the flow details remain to be clarified by future experiments.

Our comparative numerical study shows several features which do not seem to be dependent on the turbulence model adopted: (i) the absence of concentration double peaks in the developed stage, in contrast with the bifurcated scalar field one often assumes in the bent-over jet in crossflow; (ii) the diffusion of turbulence energy and passive scalar into the wake; (iii) the generation of vorticity tails of opposite orientation in the puff rear, due to spatial inhomogeneities in the turbulent viscosity. Nevertheless, the RNG model computes a much stronger stagnation region and concentration appendix in the puff rear. The present results also suggest that streamline curvature effects (or high strain rates) around the vortex cores, which may not be described adequately by the standard model, play a relatively minor role as far as the major puff mixing characteristics are concerned. The puff flow is mainly governed by the large-scale motion as implied by the similarity relations.

ACKNOWLEDGEMENTS

This work was carried out while the second author was a visiting research fellow at the University of Hong Kong. The project was supported by the Hong Kong Research Grants Council and in part by a grant from the National Science Foundation of China. All computations were performed on an IBM RISC System/6000 (3BT) workstation. It is also appropriate to note that the numerical simulation on line puffs was originally supported by an Alexander von Humboldt Research Fellowship granted to the first author.

REFERENCES

1. R.S. Scorer, *Environmental Aerodynamics*, Ellis Horwood, Chichester, 1978.
2. H.B. Fischer *et al*., *Mixing in Inland and Coastal Waters*, Academic, New York, 1979.
3. J.H.W. Lee, W. Rodi and C.F. Wong, 'Turbulent momentum line puffs', *ASCE J. Engng. Mech*., **122**, 19–29 (1996).
4. J.M. Richards, 'Puff motions in unstratified surroundings', *J. Fluid Mech*., **21**, 97–106 (1965).
5. V.H. Chu and M.B. Goldberg, 'Buoyant forced plumes in crossflow', *Proc. ASCE*, *J. Hydraul. Div*., **100**, 1203–1214 (1974).
6. S.J. Wright, 'Mean behavior of buoyant jet in a crossflow', *Proc. ASCE*, *J. Hydraul. Div*., **103**, 499–513 (1977).
7. C.S. Yih, 'Similarity solutions for turbulent jets and plumes', *ASCE J. Engng. Mech*., **107**, 455–478 (1981).
8. Yakhot *et al*., 'Renormalization group analysis of turbulence, I. Basic theory', *J. Sci. Comput*., **1** 1–51 (1986).
9. G.K. Batchelor, *An Introduction to Fluid Dynamics*, Cambridge University Press, Cambridge, 1967.
10. R.I. Sykes *et al*., 'On the vorticity dynamics of a turbulent jet in a crossflow', *J. Fluid Mech*., **168**, 393–413 (1986).
11. S.V. Patankar, *Numerical Heat Transfer and Fluid Flow*, Hemisphere, New York, 1980.
12. *FLUENT (Version 4.3) User's Guide*, Fluent Inc., Lebanon, NH, 1995.

© 1998 John Wiley & Sons, Ltd.

13. B.P. Leonard, 'A stable and accurate convective modelling procedure based on quadratic upstream interpolation', *Comput. Meth. Appl. Mech. Engng.*, **19**, 59–98 (1979).
14. J.P. Van Doormaal and G.D. Raithby, 'Enhancement of the SIMPLE method for predicting incompressible fluid flows', *Numer. Heat Trans.*, **7** 147–163 (1984).
15. A. Glezer and D. Coles, 'An experimental study of a turbulent vortex ring', *J. Fluid Mech.*, **211**, 243–283 (1990).
16. V.H. Chu, 'Oblique turbulent jets in a crossflow', *ASCE J. Engng. Mech.*, **111**, 1343–1360 (1985).
17. J.S. Turner, 'Turbulent entrainment: the development of the entrainment assumption, and its application to geophysical flows', *J. Fluid Mech.*, **173**, 431–471 (1986).
18. G. Tsang, 'Laboratory study of line thermals', *Atmos. Environ.*, **5**, 445–471 (1971).
19. J.M. Richards, 'Experiments on the motions of isolated cylindrical thermals through unstratified surroundings', *Int. J. Air Water Pollut.*, **7**, 17–34 (1963).
20. W. Rodi, *Turbulence Models and Their Application in Hydraulics*, IAHR, Delft, 1980.

© 1998 John Wiley & Sons, Ltd.